Viscoelastic properties of marginal networks in a solvent

M. Dennison and H. Stark
Institut für Theoretische Physik, Technische Universität Berlin, Hardenbergstrasse 36, 10623 Berlin, Germany
(Received 6 November 2015; published 16 February 2016)

Polymer networks at the margins of mechanical stability are known to be highly sensitive to applied forces and fields and to exhibit an anomalously large resistance to deformation. In this paper, we study the effects of hydrodynamic interactions on the behavior of marginal networks using a hybrid molecular dynamics and multiparticle collision dynamics simulation technique. We examine how the filament and solvent properties affect the response of marginal networks to shear. We find that the stiffening of the network shows a stronger dependence on the shear frequency when hydrodynamic interactions are present than when they are not. The network shear modulus scales as $G' \sim \omega^{\alpha_c}$, with a critical stiffening exponent α_c that can be controlled by varying the relative concentrations of the network and the solvent. Our results show that this arises due to the solvent aiding the relaxation of the network and suppressing the network nonaffinity, with the system deforming more affinely when hydrodynamic interactions are maximized.

DOI: 10.1103/PhysRevE.93.022605

I. INTRODUCTION

It has been the aim of many theoretical and simulation studies to understand how the rigidity of elastic networks is affected by both the elastic properties of the filaments making up the network and the network topology, i.e., how and where the filaments are connected [1,2]. Maxwell showed that a network of simple springs will become rigid and resist linear deformation at a critical connectivity, corresponding to the point when the number of degrees of freedom is just balanced by the number of constraints [3]. This critical point is also referred to as the marginal point, as it is here that such a network is at the margin of stability. However, networks can be stabilized at and below the marginal point if an additional interaction or force (beyond central-force interactions) is present in the system. For example, it has been shown that mechanically floppy networks can resist deformation if the polymers have a bending stiffness [4,5], if molecular motors are present [6–8], or due to thermal fluctuations [9,10]. In these systems the network will become floppy at a second, lower critical point, at which a single connected path spanning the network will enable it to resist deformation [11,12]. Indeed, rigidity percolation models also exhibit critical behavior, often as a function of connectivity [11–15].

Beyond simply marking the onset of mechanical stability, marginal networks at the critical point are theoretically predicted to have many interesting and potentially useful properties. For instance, marginal networks can exhibit an anomalously large rigidity and have a highly tunable elastic behavior that depends both on the constituent filament properties and on the additional stabilizing interaction [4,7,9]. One aspect of the behavior of marginal networks that is not yet well understood, and which would be of importance to experimental studies, is their dynamical behavior in the presence of a solvent. Numerous studies have examined the dynamics of networks far from the marginal point [16–23], where the stiffening of a network with an applied shear frequency was shown to exhibit an $\omega^{0.75}$ dependence. This behavior is believed to be universal for all stiff biopolymer networks [20]. There has also been much interest in the dynamical behavior of systems of jammed-particle packings at the verge of mechanical stability [24–27]. However, little is known about how marginal networks are affected by the presence of hydrodynamic interactions mediated by flow fields, which the network generates during motion. By assuming a viscous coupling between the network nodes and a uniformly sheared liquid, Ref. [28] showed that a viscous drag acts like a field taking the system away from criticality, as it can dampen the nonaffine fluctuations that give rise to stiff marginal networks [27]. In both studies, hydrodynamic interactions mediated by the solvent were neglected. Such considerations can be important: networks that are strongly coupled to a solvent, due to, for example, a high fluid viscosity, a small mesh size of the network, or a high frequency of the applied deformation, take on the incompressible nature of the fluid and their motion becomes highly correlated to that of the solvent [29,30]. Conversely, networks can be considered as compressible even in an incompressible solvent for large mesh sizes, less viscous solvents, or for low-frequency deformations, where the fluid flow can pass relatively unhindered through the network pores and hence the solvent and the network exhibit a high degree of relative motion. This can lead to a crossover in the behavior of biopolymer networks from a nonaffine to an affine response [31].

In this work, we study the effects of hydrodynamic interactions on the viscoelastic response of two-dimensional (2D) spring networks above, below, and at the marginal point. We examine how the solvent affects the system as a function of both the network and solvent properties when an oscillating shear strain is applied. Our results show that hydrodynamic interactions have the effect of making marginal networks more compliant to shear. This is due to the network deforming more affinely in response to the applied deformation.

II. METHODS

We consider two-dimensional triangular lattice-based networks. To form these networks, which have been used in many previous studies [4,6,9,28,32,33], we place N nodes on lattice sites and connect nearest-neighbor nodes by N_s model filament segments. In order to obtain a desired network connectivity $z = 2N_s/N$, which is the average coordination

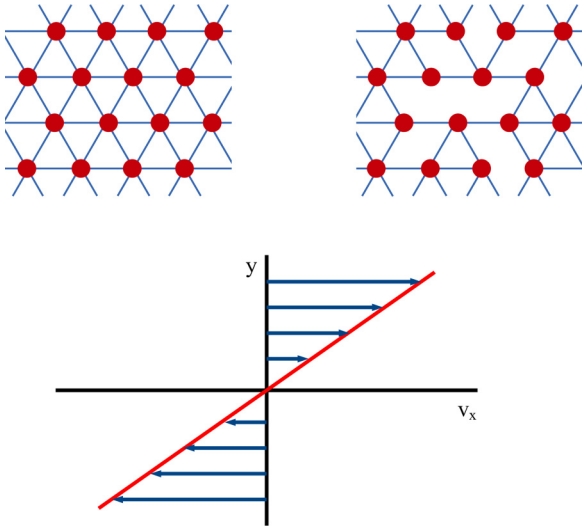

FIG. 1. Top: Example of triangular lattice-based networks. Lines indicate filaments, which are connected at network nodes, indicated by the red circles. Left shows a fully connected network with connectivity $z = 6$, right shows a diluted network ($z < 6$), where random filament segments have been removed. Bottom: Schematic representation of the typical pure-fluid flow field (i.e., no network is present) when the system is sheared, in the v_x-y representation, where y is the height through the simulation box and v_x is the average velocity in the x direction.

number of the nodes, we remove randomly chosen segments until a target connectivity is reached. During the simulations the nodes are allowed to fluctuate off lattice. Sections of both a fully connected and a randomly diluted network are shown in Fig. 1. As the networks are diluted randomly, finite-size effects can be important, with different realizations exhibiting slightly different values for the critical connectivity z_c, the point at which the network is just mechanically stable [4]. In order to minimize these, we simulate relatively large networks of $N = 100 * 100$ nodes. In addition, we average all our results over multiple network realization sets. Each realization set is where we gradually dilute a fully connected lattice to progressively lower connectivities.

We model the filaments making up the network as Hookean springs of length ℓ, rest length ℓ_0 (corresponding to the lattice spacing) and spring constant $k_{\rm sp}$, for which the spring energy U is given by

$$U = \frac{k_{\rm sp}}{2}(\ell - \ell_0)^2. \tag{1}$$

The springs, which are freely hinged at the nodes and can stretch indefinitely, are treated as phantom, i.e., we allow them to overlap.

We use a hybrid molecular dynamics (MD) and multiparticle collision dynamics (MPCD) simulation technique, which allows for hydrodynamic interactions within the network, as well as network thermal fluctuations, to be incorporated. The dynamics of the network is modeled using a standard MD simulation scheme, while the MPCD technique is used to simulate the solvent. The MPCD technique (also known as stochastic rotation dynamics), which efficiently solves the Navier-Stokes equation, was first proposed by Malevanets and Kapral [34], and has since been successfully used to study a diverse range of soft-matter and biological systems, such as colloids [35,36], active particles [37], vesicles and cells [38], bacterial flagella [39], polymers [40,41], and sheets [42] (for an overview of the technique see Refs. [43,44]).

In the MPCD technique the solvent is modeled by a large number of fictitious, point fluid particles, and their dynamics is conducted in two steps. In the so-called streaming step the fluid particles move ballistically for a set time interval, while in the collision step they are coarse grained into cells in which they interact with each other according to a predefined collision rule. We use the MPC-AT algorithm, where the Anderson thermostat is employed and the average thermal energy of the system is kept at $k_B T$ during the collision step [43]. Allowing the fluid particles to interact and exchange momentum only in the collision step is the origin of the method's computational efficiency. As long as the collision rule conserves the mass and momentum at the local level, i.e., within a cell, the correct hydrodynamic flow field will be recovered. The coupling of the network to the solvent in this scheme can be carried out in the collision step, where the network nodes are also treated as fictitious particles and included in the collision step, in the same manner as for polymers in Refs. [40,41,45]. We note that in the MPCD method the spring rest length ℓ_0 (corresponding to the lattice spacing) should not be much smaller than the MPCD cell size a, in order that hydrodynamic interactions between network nodes are well resolved [43].

The viscosity η of the solvent is controlled by varying the number of fluid particles n_f and/or the time step between collisions ∂t_c. Its value can be determined either analytically [43] or numerically [46]. The analytic predictions differ from the numeric results at low values of ∂t_c, and hence we have used numeric predictions. However, we find that the choice of numeric or analytic value does not qualitatively affect our findings.

We deform the networks by applying a time-dependent shear strain using Lees-Edwards boundary conditions [47]. The strain $\gamma(t)$ oscillates in time t with a frequency ω and is given by

$$\gamma(t) = \gamma_0 \sin(\omega t), \tag{2}$$

where γ_0 is the amplitude. In order to shear the network, the shear strain is applied to all springs crossing the boundary of the simulation box, such that their spring energy is modified to become [9,28]

$$U = \frac{k_{\rm sp}}{2}\left(\left\{[x_{12} - \gamma(t)L]^2 + y_{12}^2\right\}^{1/2} - \ell_0\right)^2, \tag{3}$$

where x_{12}, y_{12} are the x, y separations of the two ends of the spring (with $\ell = [x_{12}^2 + y_{12}^2]^{1/2}$ for springs not crossing the boundary) and L is the height of the simulation box.

A solvent sitting between two parallel plates in a rheometer will also experience the effects of shearing, and to take this into account we again employ Lees-Edwards boundary conditions. The velocity v_j and position r_j of a fluid particle j crossing the top or bottom of the simulation box is modified to become [47]

$$\begin{aligned} r_j &= r_j + I_L \gamma(t) L \partial t, \\ v_j &= v_j + I_L \gamma(t) L, \end{aligned} \tag{4}$$

where $I_L = -1$ if the particle crosses the upper boundary and $I_L = 1$ if it crosses the lower boundary, and ∂t is the simulation time step. Figure 1 shows a schematic of the fluid flow field when this shear is applied, in the absence of a network. In practice, we find that applying a shear to the fluid has little effect on the response of the network, as the motion of the fluid appears to become dominated by interactions with the network rather than by the shear acting directly on it.

After shearing the system, we can then calculate the corresponding shear stress $\sigma(t)$ as in previous work [9,28], to which we fit the following function

$$\sigma(t) = \sigma_0 \sin(\omega t + \delta), \tag{5}$$

to extract the stress amplitude σ_0 and the phase lag δ. The dynamical shear modulus G^* can then be calculated as

$$\begin{aligned} G^* &= G' + iG'', \\ &= \frac{\sigma_0}{\gamma_0}[\cos(\delta) + i\sin(\delta)], \end{aligned} \tag{6}$$

where the real part G' represents the storage modulus and the imaginary part G'' is the loss modulus [28].

We note that we can accurately find the critical connectivity z_c for each network realization set by calculating the linear shear modulus G_0 as a function of z using the conjugate gradient method, as in many previous studies (see, e.g., Ref. [4]). This enables us to find the connectivity at which G_0 vanishes, corresponding to z_c. We also note that the two main energy scales in our simulations are the mechanical energy of the springs, given by $k_{sp}\ell_0^2$, and the thermal energy k_BT. We therefore define the dimensionless reduced temperature

$$T^* = k_BT/k_{\rm sp}\ell_0^2, \tag{7}$$

which measures the ratio of the two. For low values of T^*, thermal fluctuations are small compared to the mechanical stretch (or compression) energy of the springs.

III. RESULTS

We have calculated the dynamical shear modulus G^* for a range of network connectivities z, shear frequencies ω and solvent viscosities η. In Fig. 2(a) we show the storage modulus G' against a reduced shear frequency $\omega^* = \omega\eta/k_{\rm sp}$ for a range of z values at a fixed reduced temperature $T^* = 10^{-6}$ [see Eq. (7)]. The low value we have chosen represents a regime where the mechanical energy is dominant over the thermal energy. However, as we shall show later, this parameter does not directly effect the stiffening of the network due to the applied shear. We have used a network with $N = 100 * 100 = 10^4$ nodes and $n_f = 10$ fluid particles per cell. The fluid mass is set to $m_f = 1$ and we note that throughout the Schmidt number $S_c \gg 1$, meaning that the fluid is in the liquidlike rather than gaslike regime [44]. We initially set the network node mass such that the network is buoyant, with the ratio of densities $m_n\rho/n_fm_f = 1$, where ρ is the number density of network nodes. We also set the rest length to be equal to the MPCD cell size $\ell_0 = a$.

The behavior of such networks in the $\omega^* \to 0$ limit has been studied previously in Ref. [9], where the linear shear modulus G_0 was found to depend on either the spring constant (above the critical connectivity, $z > z_c$), the temperature (for $z < z_c$), or both (for $z \sim z_c$). For all networks we indeed see an initial constant storage modulus at sufficiently low ω^*, which is equal to the linear shear modulus $G' = G_0$ [shown only for $z \gtrsim z_c$ in Fig. 2(a)]. As ω^* increases the networks begin to stiffen, with the modulus scaling as $G' \sim (\omega^*)^\alpha$ where α takes one of two values depending on z, consistent with results of Ref. [28]. For $z < z_c$ the networks stiffen with $\alpha = 2$, as in Ref. [28].

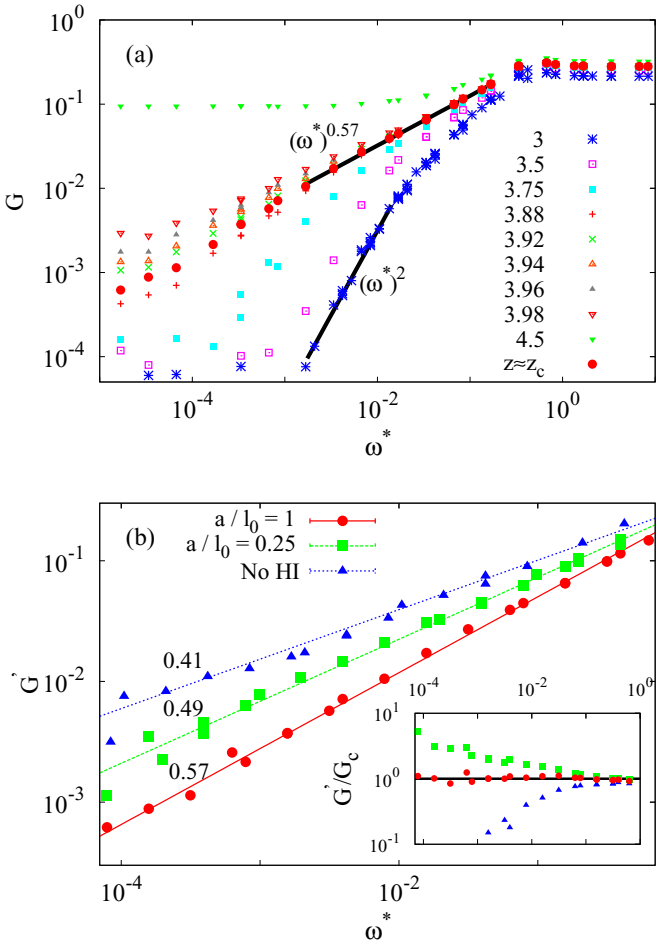

FIG. 2. (a) Storage modulus G' (in units of the spring constant $k_{\rm sp}$) against $\omega^* = \omega\eta/k_{\rm sp}$ for 2D triangular lattice-based Hookean spring networks, where ω is the shear frequency and η the solvent viscosity. Connectivity of the network is indicated by different symbols (critical connectivity $z_c \sim 3.891$). Lines indicate ω^* dependencies. (b) Stiffening of networks at $z \sim z_c$ with two different values of the spring rest length ℓ_0 (in units of the MPCD cell size a), as indicated in the legend. No HI indicates a system where hydrodynamic interactions are neglected. Lines indicate a fit of the form $G_c \sim (\omega^*)^{\alpha_c}$, with the α_c values given in the plot. Here the parameter X [see Eq. (8) and Eq. (9)] is: $X \sim 0.4$ (circles), corresponding to relatively dense networks, $X \sim 0.01$ (squares), corresponding to a less dense network, and $X = 0$ (triangles), corresponding to a vanishingly sparse network. Inset: G'/G_c against ω^*, where $G_c \sim (\omega^*)^{\alpha_c}$ is the function fitted to the above data for a network at the critical point, with $\ell_0/a = 1$. Symbols indicate network connectivity: $z = 4.2$ (squares), $z \sim z_c \sim 3.891$ (circles), and $z = 3.7$ (triangles). All data is at reduced temperature $T^* = k_BT/k_{\rm sp}\ell_0^2 = 10^{-6}$, where T is the temperature, k_B the Boltzmann constant, and ℓ_0 the spring rest length.

At the critical connectivity z_c the network stiffens with a critical stiffening exponent $\alpha_c \sim 0.57$. This behavior is found over many orders of magnitude of ω^*, as shown in the inset of Fig. 2. This differs substantially from the value $\alpha_c \sim 0.41$ that was found in Ref. [28], where hydrodynamic interactions were neglected but where a friction term was used to approximate the viscous drag arising due to the solvent. It also differs from the high-frequency $G' \sim \omega^{0.75}$ behavior found for biopolymer networks [19,20,29]. Such a difference implies that hydrodynamic interactions cause a more rapid stiffening of the network as ω^* is increased. However, the network will also be softer, since a higher stiffening exponent will result in a lower G' at $\omega^* \ll 1$. This can be seen in Fig. 2(b) where we compare the observed behavior to an identical system where hydrodynamic interactions are neglected. This can be done as in Ref. [28], or using the MPCD technique, where randomly interchanging the solvent velocities results in a system with a viscous drag but no hydrodynamic flow field [48]. Both techniques give the same value of $\alpha_c \sim 0.41$. We also note that, as in Ref. [28], the loss modulus also scales as $G'' \sim (\omega^*)^{\alpha_c}$ (not shown).

In order to qualitatively examine this effect, we determine α_c for systems with the same solvent properties as before, but now with different values of the ratio of MPCD cell size to spring rest length, a/ℓ_0. As Fig. 2(b) and Fig. 3(a) shows, for small values of a/ℓ_0 the network stiffens with a relatively small exponent, which then increases with a/ℓ_0. When a/ℓ_0 is small, hydrodynamic interactions become effectively smaller as the network nodes are sufficiently far apart that the interactions mediated via the solvent are weaker, and thus our system becomes more like that of Ref. [28]. As a/ℓ_0 increases the network nodes become closer and hydrodynamic interactions between nodes are therefore larger.

As noted previously, it is not possible to study values of a/ℓ_0 much greater than 1 in the MPCD method [43]. However, this behavior raises the question of how α_c is affected by changes in other parameters of the solvent and network, which affect the strength of the hydrodynamic interactions. If we consider the interaction between the fluid and network using the MPCD technique, the influence that the network has on the fluid particles can be expected to be related to the relative momentum densities of the network and the fluid inside of a cell. That is,

$$X = \frac{\rho_n \langle v_n \rangle}{\rho_f \langle v_f \rangle} = \frac{1}{n_f}\left(\frac{a}{\ell_0}\right)^2 \sqrt{\frac{m_n}{0.75 m_f}}, \tag{8}$$

where $\langle v_{n,f} \rangle = (k_B T/m_{n,f})^{0.5}$ is the average velocity of a node or fluid particle, where we take the velocities of the network nodes and fluid particles to be dominated by thermal fluctuations, which is the case in the stiffening regime. Here $\rho_n = m_n/\sqrt{0.75}\ell_0^2$ is the mass density of the network and $n_f m_f/a^2$ is that of the solvent. The bottom line of this expression is specific for the parameters of the MPCD simulation method. The top line would, however, also be true for any interaction we could use in our simulations where the network and solvent exchange momentum, e.g., via collisions using an MD simulation scheme. We can also rewrite it in terms of the parameters of a physical system. That is,

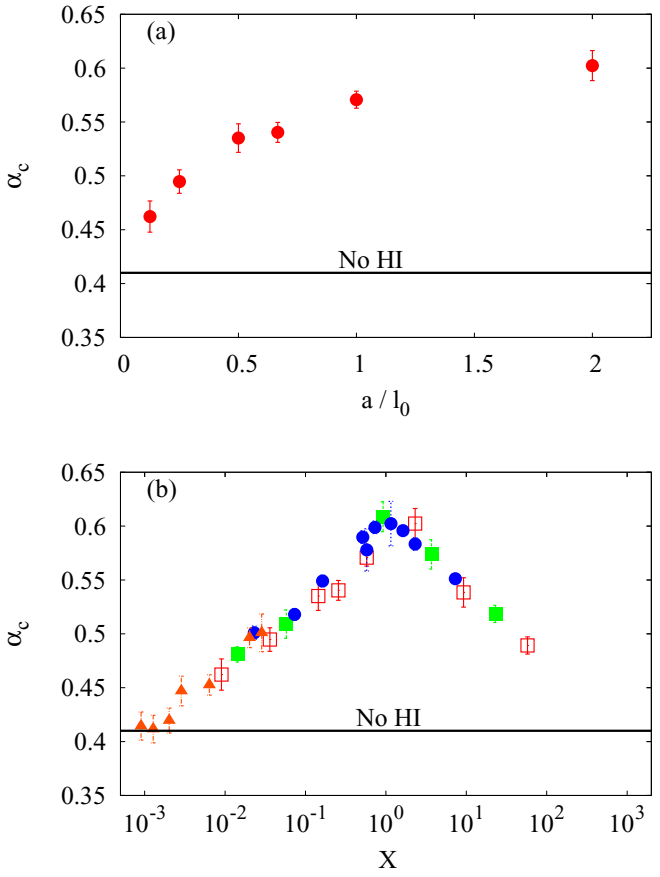

FIG. 3. (a) Critical stiffening exponent α_c against the ratio of MPCD cell size to spring rest length a/ℓ_0, for networks with $n_f = 10$ fluid particles per cell and ratio of node to fluid particle densities $m_n\rho/n_f m_f = 1$. (b) α_c against X, the ratio of network to fluid momentum densities [see Eq. (8)]. Different symbols represent data obtained for various combinations of n_f, $m = m_n/m_f$ and ℓ_0/a values: $m = 10$, $n_f = 2$ (open squares), $m = 10$, $n_f = 10$ (solid squares), $\ell_0/a = 0.5$, $n_f = 2$ (open circles), $\ell_0/a = 1$, $n_f = 50$ (solid circles), $\ell_0/a = 0.5$, $n_f = 10$ (open triangles), $\ell_0/a = 8$, $n_f = 50$ (solid triangles). Solid horizontal lines (labeled NO HI) show the value predicted when hydrodynamic interactions are absent.

$$X = \frac{c_n}{c_f}\left(\frac{M_f}{M_n}\right)^{0.5}, \tag{9}$$

where c_n and c_f are the mass concentrations of the network and the fluid, and M_f and M_n are the molar masses of the fluid and of the polymers making up the network, respectively. Here and above we make the assumption that the motion of the nodes in the network is thermal. This may not always be the case, but it allows us to make a rough estimate of X for experimental systems. In an experimental system, c_f, M_f, and M_n are typically fixed, while the network concentration c_n (i.e., the concentration of polymers in the fluid) can be varied, as in the experimental studies of Refs. [49–51]. In these systems, the ratio c_n/c_f can be in the range $\sim 10^{-3}$–10^{-1}, while M_n/M_f can be in the range $\sim 10^3$–10^5.

We now calculate α_c for systems with a range of $m = m_n/m_f$, ℓ_0/a, and n_f values, plotting them against X in

Fig. 3(b). Here we see that $\alpha_c \sim 0.41$ for low X values, consistent with Ref. [28] in the limit of vanishing hydrodynamic interactions at $X \to 0$. Physically this can be thought of as a dilute network, where $c_n \ll c_f$. As X is increased, α_c increases and reaches a peak of $\alpha_c \sim 0.6$ close to $X = 1$, before it then decreases again for $X > 1$. The curve appears to be symmetric about $X = 1$ [Fig. 3(b)], although it is not possible to determine the value of α_c as X approaches the artificial limit $X \to \infty$ with our current data. We can, however, identify three regimes of behavior for α_c. When the network is dilute, $X \to 0$ and the system stiffens with $\alpha_c \sim 0.41$. Here the network is much less dense than the solvent, and either the nodes are sufficiently separated that they do not interact with each other via the solvent, or the nodes lack the momentum to influence the dynamics of the solvent. At $X \sim 1$ hydrodynamic interactions are maximized and α_c becomes larger. Typically $\omega^* \ll 1$ combined with a larger exponent corresponds to a softer network. Finally, for artificial limit $X > 1$ the solvent is less dense than the network. In this regime, while we expect network nodes to have a large influence on the dynamics of the fluid, the fluid has little influence on the nodes. Again, this minimizes hydrodynamic interactions and decreases α_c, resulting in a stiffer network.

To understand where experimental systems that have the potential to form marginal networks would sit in Fig. 3, we can use Eq. (8) to calculate X for networks of semiflexible polymers. While our results are in two dimensions, we expect a similar peak at $X \sim 1$ as in Fig. 3 in three dimensions. The semiflexible synthetic networks of Ref. [49], which have been shown to exhibit critical behavior in their response to stress [50,51], have a value of $X \sim 10^{-4}$–10^{-3} in water, well below the peak value and close to where we expect stiffer networks with low α_c. For biopolymer networks consisting of neurofilaments, for example, we estimate $X \sim 10^{-2}$–10^{-1} in water [49], which should show some of the effects of hydrodynamic interactions [see Fig. 2(b) where we compare networks with $X \sim 10^{-2}$ to those with $X = 0$], if a marginal state could be achieved.

Clearly, hydrodynamic interactions have the effect of making a marginal network less stiff via increasing the critical stiffening exponent α_c. In order to understand how this happens, we examine the differential nonaffinity of the network as it is deformed. The differential nonaffinity measures how nonaffine the response of the network is to an applied deformation, and is defined as [28]

$$\Gamma = \frac{1}{\ell_0^2}\frac{\partial^2}{\partial\gamma^2}\langle(\mathbf{r}_{na} - \mathbf{r}_a)^2\rangle. \tag{10}$$

Here, $\mathbf{r}_{na}$ is the position of a node and $\mathbf{r}_a$ is the position if the displacement would have been affine (so $\mathbf{r}_{na} - \mathbf{r}_a$ is the nonaffine contribution to the displacement), and $\langle \dots \rangle$ denotes the average over all nodes. A high value of Γ means that the network deformation is highly nonaffine, while a low value means it is more affine. It has been shown that the nonaffinity of a marginal network's response is crucial to its unusual behavior [4,7,28]. Furthermore, at z_c the shear modulus scales as $G' \sim \Gamma\omega^* \sim (\omega^*)^{\alpha_c}$, where the nonaffinity couples to the applied shear deformation, causing the unusual stiffening behavior observed in Ref. [28]. At z_c the nonaffinity scales as $\Gamma \sim (\omega^*)^{-\beta_c}$ where the relation $\alpha_c + \beta_c = 1$ was found in Ref. [28] by estimating the power dissipated in the system both from viscous forces ($W \sim \Gamma\omega^{*2}\gamma_0^2$) and on the macroscopic level ($W = G''\omega^*\gamma_0^2/2$), such that $G'' \sim \Gamma\omega^*$ and hence $G' \sim \Gamma\omega^*$. Thus if β_c is increased, α_c would decrease and we would have a stiffer network. Conversely, if β_c is decreased, α_c increases and the network is less stiff. We calculate Γ for the networks studied above and we indeed find that $\alpha_c + \beta_c = 1$ holds in all cases. An example of this behavior is shown in Fig. 4. Thus, hydrodynamic interactions have the effect of increasing the nonaffinity of a marginal network's response to shear (via lowering β_c), which results in a network that is less stiff than it would be in their absence.

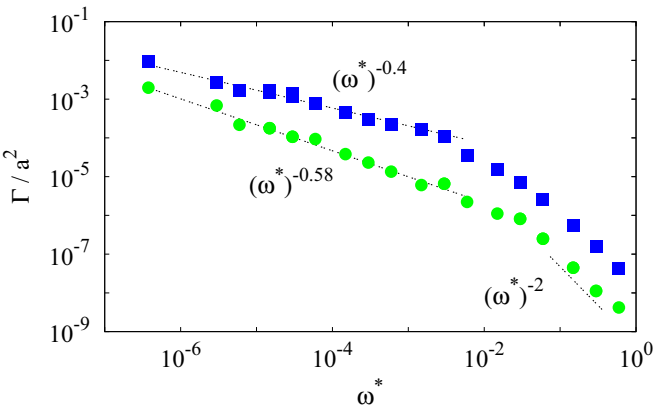

FIG. 4. Differential non-affinity Γ against reduced shear frequency ω^* for Hookean spring networks at reduced temperature $T^* = k_B T/k_{sp}\ell_0^2 = 10^{-6}$. Squares show a network with $\ell_0/a = 1$, $m = m_n/m_f = 20$ and $n_f = 5$ ($X \sim 1$, $\alpha_c \sim 0.6$). Circles show a network with $\ell_0/a = 8$, $m = m_n/m_f = 10.0$ and $n_f = 20$ ($X \sim 0.003$, $\alpha_c \sim 0.42$). Dashed lines show frequency dependence.

To gain a better understanding of this change in the critical stiffening exponent α_c, we make use of a scaling ansatz, which has been shown to capture the different regimes of network behavior under shear. That is, the storage modulus G' may be expressed as [27,28]

$$G' \sim |\Delta z|^f k_{sp}\mathscr{F}_\pm\left(\frac{\omega^*}{\omega_0^*}\right), \tag{11}$$

where $\Delta z = z - z_c$, $\mathscr{F}_+(x)$ is a function which describes the network behavior above z_c and $\mathscr{F}_-(x)$ describes it below. The crossover frequency ω_0^* is the highest shear frequency at which the network can fully relax, i.e., at which it relaxes from the initial, affinely deformed, state to the relaxed state it would assume at $\omega^* \to 0$, where the free energy would be minimized. It has been shown empirically that ω_0^* exhibits power-law behavior, with $\omega_0^* \sim |\Delta z|^\phi$ [27,28], from which we can write

$$G' \sim |\Delta z|^f k_{sp}\mathscr{F}_\pm\left(\frac{\omega^*}{|\Delta z|^\phi}\right), \tag{12}$$

where f and ϕ are critical exponents. f arises from the behavior of the linear shear modulus G_0 of an athermal network as the connectivity is lowered from $z = 6$ to z_c. As this is invariant to the applied shear frequency, $\mathscr{F}_+(x) \sim x^0$ and hence $G_0 \sim |\Delta z|^f k_{sp}$. G_0 may be calculated very accurately

via a conjugate gradient method, and from this we find that value of $f \sim 1.4 \pm 0.02$ gives a good fit to simulation data, both here and in previous work [4,9,28].

This leaves the parameter ϕ as the only unknown in Eq. (12), and there are two methods by which we can determine it. First, we may simply vary it in order to visually find the best collapse of the data. However, in order to minimize the errors in our estimate, which can be large for critical exponents [52], we consider the function $\mathscr{F}_-(x)$, which describes the network stiffening behavior below z_c. This scales as $\mathscr{F}_-(x) \sim x^2$, as for a Maxwell fluid. From Eq. (12) this gives $G' = c|\Delta z|^{f-2\phi} k_{\rm sp} (\omega^*)^2$, where c is a constant. By fitting the function

$$G' = C(z) k_{\rm sp} (\omega^*)^2, \tag{13}$$

where $C(z) = c|\Delta z|^{f-2\phi}$ is a constant, which varies with z, to data for systems below the critical connectivity, we may extract ϕ. By doing so, we minimize the errors in ϕ, as opposed

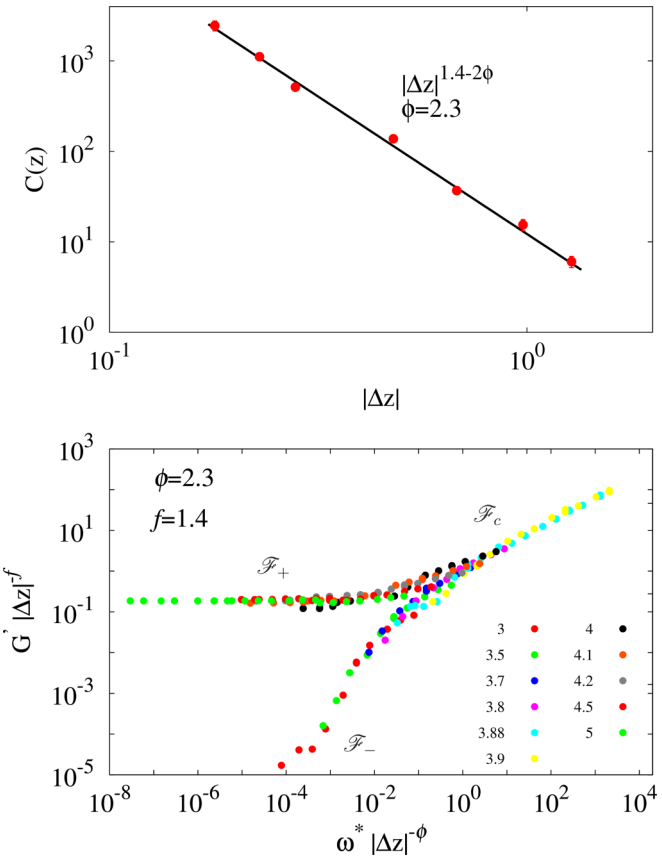

FIG. 5. (a) $C(z) = c|\Delta z|^{f-2\phi}$ as a function of distance from the critical point $|\Delta z| = |z - z_c|$ [see Eq. (13)]. Solid line indicates a fit to the data, from which ϕ may be accurately extracted. (b) Storage modulus G' as a function of $\omega^* = \omega\eta/k_{\rm sp}$ and $|\Delta z|$, the distance from the critical connectivity, for Hookean spring networks. All data is at reduced temperature $T^* = k_B T/k_{\rm sp}\ell_0^2 = 10^{-6}$, where T is the temperature, k_B the Boltzmann constant, k the spring constant and ℓ_0 the spring rest length. Data shown here is for a system with $\ell_0/a = 1$, $m = m_n/m_f = 10$ and $n_f = 5$ ($X = 0.73$), and is scaled using the ansatz in Eq. (12). A range of connectivities have been used, indicated in the legend. The critical connectivity is $z_c \sim 3.891$, $f \sim 1.4$ and $\phi \sim 2.3 \pm 0.1$ [taken from (a)]. Modulus is in units of $k_{\rm sp}$.

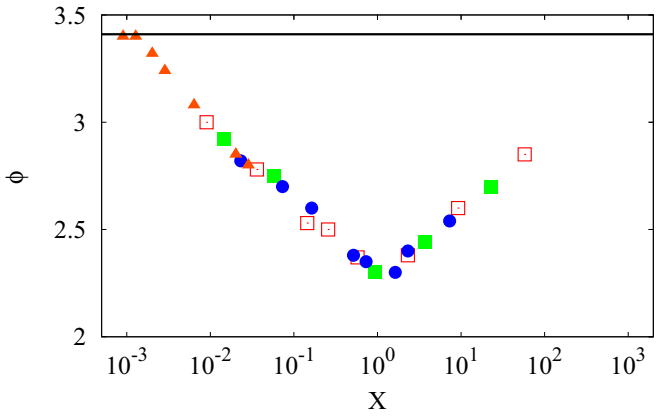

FIG. 6. Critical exponent ϕ as a function of X, the ratio of network to fluid momentum densities [see Eq. (8)]. ϕ gives the scaling of the critical relaxation frequency $\omega_0^* \sim |\Delta z|^\phi$ with the distance from the critical point $|\Delta z|$. Different symbols represent data obtained for the combinations of n_f, m and ℓ_0/a values as in Fig. 3.

to simply varying it to find the best collapse of our data. An example of this is shown in Fig. 5(a). We then use this to collapse the data presented in Fig. 2, which is shown in Fig. 5(b). Here we use $f \sim 1.4$ and $\phi \sim 2.3 \pm 0.1$.

Three branches of network response can be seen: a branch described by $\mathscr{F}_+(x)$, which is independent of ω^*, such that $\mathscr{F}_+(x) \sim x^0$; a branch described by $\mathscr{F}_-(x)$, which scales as $(\omega^*)^2$, such that $\mathscr{F}_-(x) \sim x^2$; and finally, a critical branch, given by $\mathscr{F}_c(x) \sim x^{\alpha_c}$. Here, $\mathscr{F}_c(x) \sim x^{f/\phi}$, and $\alpha_c = f/\phi$. This relation between the critical stiffening exponent α_c and the critical exponents f and ϕ is due to the fact that at $|\Delta z| = 0$ the storage modulus must become independent of Δz, since it is neither 0 or ∞ for finite ω^*. This can only be satisfied if $\alpha_c = f/\phi$. Interestingly, this scaling collapse also shows that a network does not have to be tuned to the critical connectivity in order to exhibit critical stiffening. Data for networks at $z = z_c$ would be at infinity on the x axis of Fig. 5, and hence the data seen in the critical branch is for networks above and below z_c. The frequency of the applied shear can take sub- and supermarginal networks into the critical regime, where they stiffen as $(\omega^*)^{\alpha_c}$.

The exponent f is an athermal, nondynamical property, and is hence fixed regardless of the properties of the solvent. However, we find that for different values of the parameter X, the ratio of network to solvent momentum densities, ϕ varies continuously, as shown Fig. 6. We find that ϕ is minimized at $X = 1$, consistent with the fact that $\alpha_c = f/\phi$ assumes its maximum value at the same point. If we then consider that the crossover relaxation frequency scales as $\omega_0^* \sim |\Delta z|^\phi$, and that close to the critical point $|\Delta z|$ is very small, it is clear that a small value of ϕ results in a larger relaxation frequency. That is, when hydrodynamic interactions are maximized, the relaxation of marginal networks from their sheared state to the minimum free-energy state is enhanced. This in turn increases the critical stiffening exponent of the system, which makes the network less stiff [see Fig. 2(b)]. Thus one may control the response of the network to an applied dynamical shear by varying the parameter X, which could be done, for example, by varying the network concentration c_n [see Eq. (9)].

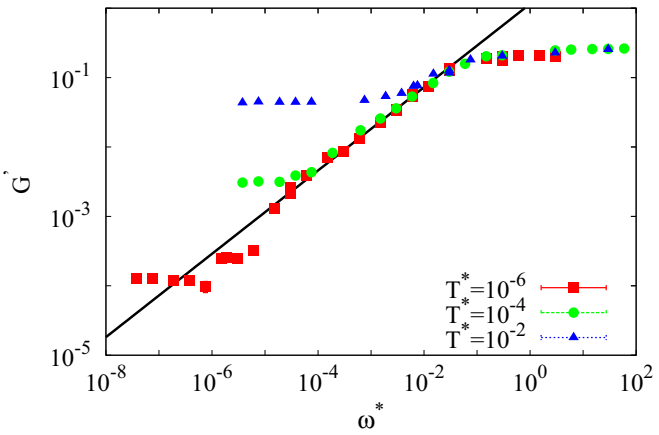

FIG. 7. MPCD-MD simulation results for storage modulus G' (the real part of the dynamical shear modulus G^*) against $\omega^* = \omega\eta/k_{sp}$, the product of shear frequency and solvent viscosity normalized by the spring constant, for 2D triangular lattice-based Hookean spring networks at a range of reduced temperatures $T^* = k_B T/k_{sp}\ell_0^2$, where T is the temperature, k_B the Boltzmann constant, k the spring constant and ℓ_0 the spring rest length. Legend indicates the value of T^*. Here $z = 3.88$, just below the critical connectivity $z_c \sim 3.891$. Modulus is in units of k_{sp}. Shading of the symbols indicates the viscosity η.

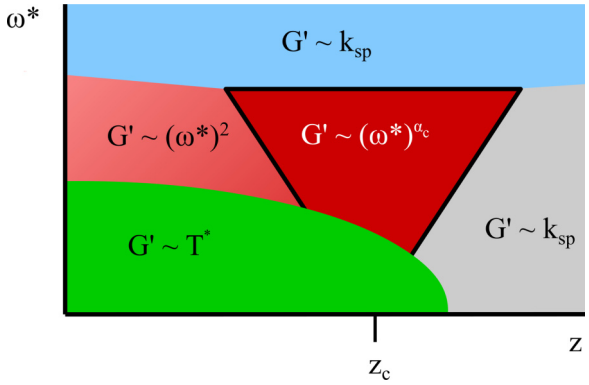

FIG. 8. Schematic diagram showing regimes of different stiffening behavior for Hookean spring networks in the z-ω^* representation, where z is the connectivity and ω^* is the reduced shear frequency $\omega^* = \omega\eta/k_{sp}$. z_c denotes the critical point of marginal connectivity. The size of the temperature-dependent regime will vary depending on the value of the reduced temperature T^*, with no such regime for $T^* = 0$, and a regime that suppresses the marginal regime as $T^* \to 1$.

We finally consider the effects of varying the reduced temperature $T^* = k_B T/k_{sp}\ell_0^2$. In agreement with previous work [9] we find that increasing the temperature has little effect on networks above the marginal point, but does result in an increase in the linear shear modulus G_0 for networks at and below z_c. As the networks stiffen we find that all the curves for different temperatures converge, as can be seen in Fig. 7, indicating that varying the temperature has no effect on the stiffening behavior. However, if the temperature is increased beyond a certain value, the linear shear modulus will dominate over the frequency-dependent regime, suppressing the critical behavior. This occurs when thermal fluctuations become comparable to the mechanical energy of the springs at $T^* = 1$, corresponding to the thermal energy becoming the dominant energy scale in the system. Physically, this would represent flexible polymers, where the polymer persistence length is much smaller than its contour length, $\ell_p \ll \ell_c$. This indicates that for a polymer network to exhibit the critical stiffening found here its constituent filaments should be semiflexible.

We summarize the complete behavior of these networks in a schematic regime diagram shown in Fig. 8. For networks above the critical connectivity, our results show that the network response to an applied shear is linear and depends only on the spring constant, shown in the right-hand region indicated by $G' \sim k_{sp}$. Networks at and below the critical point can be stabilized by thermal fluctuations and also exhibit a linear response regime, which scales with temperature, indicated by $G' \sim T^*$ on the left-hand side of Fig. 8. The size of this region grows as the temperature is increased, as indicated by Fig. 7. As the shear frequency is increased, submarginal networks behave as Maxwell fluids and stiffen as $G' \sim \omega^2$, while marginal networks stiffen as $G' \sim \omega^{\alpha_c}$, where we have shown that α_c will vary depending on the system parameters. Interestingly, networks that are above and below the marginal point can exhibit this critical behavior, as shown in Fig. 5 and indicated by the fanning out of the critical regime denoted by $G' \sim \omega^{\alpha_c}$. Finally, all networks enter a linear response at very high values of the shear frequency, as the network deforms affinely with the applied deformation, indicated by the top most $G' \sim k_{sp}$ region in Fig. 8.

IV. CONCLUSIONS

Using a hybrid molecular dynamics and multiparticle collision dynamics simulation technique we have shown how hydrodynamic interactions can affect the rigidity of an elastic network. Our results show that, consistent with previous work, networks on the margins of mechanical stability stiffen as $G' \sim (\omega^*)^{\alpha_c}$, with $\alpha_c < 1$. This sublinear exponent means that the network is actually relatively stiff, as $\omega^* \ll 1$. However, we have found that hydrodynamic interactions give rise to a varying stiffening exponent, which is always larger than that reported previously in a system where these interactions were neglected. This results in a network that is, in fact, less stiff.

The change in exponent is due to the hydrodynamic interactions causing the network to deform more affinely and increasing the crossover frequency at which the network can relax under dynamical shear. The critical exponent ϕ controls the crossover frequency ω_0^*, the frequency at which the network can no longer fully relax from the sheared state to its equilibrium state. As $\omega_0^* \sim |z - z_c|^{\phi}$, a smaller exponent results in a larger ω_0^* (as $|z - z_c|$ is small close to z_c), and hence a network, which is better able to relax. As $\alpha_c \propto 1/\phi$, this then increases the critical stiffening exponent, which results in a softer network.

We have shown how this effect may be quantified by the ratio of the momentum densities of the network and the solvent: when the ratio is close to unity α_c is maximized, while it is minimized when the ratio is very large or very small. Critical exponents in elastic networks such as those studied

here are usually universal for a given network topology. That is, while they can change for different network topologies (e.g., square lattice networks [53], triangular networks [9], and random-bond networks [54] all show different critical exponents when stabilized with temperature), exponents that evolve in a continuous manner such as these have, to our knowledge, not been reported (although we note that the critical exponent of a quantum phase transition has been shown to vary with the properties of the sub-Ohmic reservoir to which the system is coupled [55]). This, therefore, represents an additional control parameter for the behavior of marginal networks.

While we have studied networks in two dimensions, it is reasonable to assume that the same would hold for real networks in three dimensions, and based on our results we would expect them to be in the region where α_c is relatively small. While we have used Hookean springs as model filament's in this work, semiflexible polymers, which make up such real networks, exhibit a more complex response to stress: Hookean springs show only a linear force-extension response, while semiflexible polymers show an initial force extension, followed by a nonlinear stiffening as it is stretched towards its contour length. This effect has been shown to give rise to increasingly complex critical behavior in the stress response of marginal networks [50,51], and an open question we aim to address in future work is how using more realistic model filaments will effect the critical response found here.

ACKNOWLEDGMENTS

Funding from the Alexander von Humboldt Foundation is gratefully acknowledged.

[1] A. R. Bausch and K. Kroy, Nature Phys. **2**, 231 (2006).
[2] C. P. Broedersz and F. C. MacKintosh, Rev. Mod. Phys. **86**, 995 (2014).
[3] J. C. Maxwell, Philos. Mag. **27**, 297 (1864).
[4] C. P. Broedersz, T. C. Lubensky, X. Mao, and F. C. MacKintosh, Nature Phys. **7**, 983 (2011).
[5] O. Lieleg, M. M. A. E. Claessens, C. Heussinger, E. Frey, and A. R. Bausch, Phys. Rev. Lett. **99**, 088102 (2007).
[6] C. P. Broedersz and F. C. MacKintosh, Soft Matter **7**, 3186 (2011).
[7] M. Sheinman, C. P. Broedersz, and F. C. MacKintosh, Phys. Rev. Lett. **109**, 238101 (2012).
[8] Y. Cai, O. Rossier, N. C. Gauthier, N. Biais, M. A. Fardin, X. Zhang, L. W. Miller, B. Ladoux, V. W. Cornish, and M. P. Sheetz, J. Cell Sci. **123**, 413 (2010).
[9] M. Dennison, M. Sheinman, C. Storm, and F. C. MacKintosh, Phys. Rev. Lett. **111**, 095503 (2013).
[10] O. Farago and Y. Kantor, Euro. Phys. Lett. **52**, 413 (2000).
[11] W. Tang and M. F. Thorpe, Phys. Rev. B **36**, 3798 (1987).
[12] W. Tang and M. F. Thorpe, Phys. Rev. B **37**, 5539 (1988).
[13] S. Feng and P. N. Sen, Phys. Rev. Lett. **52**, 216 (1984).
[14] D. J. Jacobs and M. F. Thorpe, Phys. Rev. E **53**, 3682 (1996).
[15] C. Moukarzel and P. M. Duxbury, Phys. Rev. E **59**, 2614 (1999).
[16] B. Hinner, M. Tempel, E. Sackmann, K. Kroy, and E. Frey, Phys. Rev. Lett. **81**, 2614 (1998).
[17] C. P. Broedersz, M. Depken, N. Y. Yao, M. R. Pollak, D. A. Weitz, and F. C. MacKintosh, Phys. Rev. Lett. **105**, 238101 (2010).
[18] C. Storm, J. J. Pastore, F. C. MacKintosh, T. C. Lubensky, and P. A. Janmey, Nature (London) **435**, 191 (2005).
[19] B. Schnurr, F. Gittes, F. C. MacKintosh, and C. F. Schmidt, Macromolecules **30**, 7781 (1997).
[20] F. Gittes and F. C. MacKintosh, Phys. Rev. E **58**, R1241(R) (1998).
[21] T. G. Mason, T. Gisler, K. Kroy, E. Frey, and D. A. Weitz, J. Rheol. **44**, 917 (2000).
[22] J. Liu, M. L. Gardel, K. Kroy, E. Frey, B. D. Hoffman, J. C. Crocker, A. R. Bausch, and D. A. Weitz, Phys. Rev. Lett. **96**, 118104 (2006).
[23] M. M. A. E. Claessens, R. Tharmann, K. Kroy, and A. R. Bausch, Nature Phys. **2**, 186 (2006).
[24] C. Heussinger and J.-L. Barrat, Phys. Rev. Lett. **102**, 218303 (2009).
[25] E. Lerner, G. Düring, and M. Wyart, Proc. Nat. Acad. Sci. USA **109**, 4798 (2012).
[26] B. Andreotti, J.-L. Barrat, and C. Heussinger, Phys. Rev. Lett. **109**, 105901 (2012).
[27] B. P. Tighe, Phys. Rev. Lett. **109**, 168303 (2012).
[28] M. G. Yucht, M. Sheinman, and C. P. Broedersz, Soft Matter **9**, 7000 (2013).
[29] F. Gittes, B. Schnurr, P. D. Olmsted, F. C. MacKintosh, and C. F. Schmidt, Phys. Rev. Lett. **79**, 3286 (1997).
[30] F. C. MacKintosh and A. J. Levine, Phys. Rev. Lett. **100**, 018104 (2008).
[31] D. A. Head, E. Ikebe, A. Nakamasu, P. Zhang, L. G. Villaruz, S. Kinoshita, S. Ando, and D. Mizuno, Phys. Rev. E **89**, 042711 (2014).
[32] D. H. Boal, U. Seifert, and J. C. Shillcock, Phys. Rev. E **48**, 4274 (1993).
[33] D. E. Discher, D. H. Boal, and S. K. Boey, Phys. Rev. E **55**, 4762 (1997).
[34] A. Malevanets and R. Kapral, J. Chem. Phys. **110**, 8605 (1999).
[35] C. Prohm, M. Gierlak, and H. Stark, Eur. Phys. J. E **35**, 80 (2012).
[36] K. Milinković, J. T. Padding, and M. Dijkstra, Soft Matter **7**, 11177 (2011).
[37] M. T. Downton and H. Stark, J. Phys.: Condens. Matter **21**, 204101 (2009).
[38] H. Noguchi and G. Gompper, Phys. Rev. Lett. **93**, 258102 (2004).
[39] S. Y. Reigh, R. G. Winkler, and G. Gompper, Soft Matter **8**, 4363 (2012).
[40] K. Mussawisade, M. Ripoll, R. G. Winkler, and G. Gompper, J. Chem. Phys. **123**, 144905 (2005).
[41] R. G. Winkler, K. Mussawisade, M. Ripoll, and G. Gompper, J. Phys.: Condens. Matter **16**, S3941 (2004).
[42] S. B. Babu and H. Stark, Eur. Phys. J. E **34**, 136 (2011).
[43] G. Gompper, T. Ihle, D. M. Kroll, and R. G. Winkler, Adv. Polym. Sci. **221**, 1 (2009).
[44] J. T. Padding and A. A. Louis, Phys. Rev. E **74**, 031402 (2006).
[45] M. Ripoll, R. G. Winkler, and G. Gompper, Phys. Rev. Lett. **96**, 188302 (2006).

[46] R. G. Winkler and C. C. Huang, J. Chem. Phys. **130**, 074907 (2009).
[47] A. W. Lees and S. F. Edwards, J. Phys. C **5**, 1921 (1972).
[48] N. Kikuchi, C. M. Pooley, J. F. Ryder, and J. M. Yoemans, J. Chem. Phys. **119**, 6388 (2003).
[49] P. H. J. Kouwer, M. Koepf, V. A. A. Le Sage, M. Jaspers, A. M. van Buul, Z. H. Eksteen-Akeroyd, T. Woltinge, E. Schwartz, H. J. Kitto, R. Hoogenboom, S. J. Picken, R. J. M. Nolte, E. Mended, and A. E. Rowan, Nature (London) **493**, 651 (2013).
[50] M. Dennison, M. Jaspers, P. H. J. Kouwer, C. Storm, A. E. Rowan, and F. C. MacKintosh, arXiv:1407.0543.
[51] M. Jaspers, M. Dennison, M. F. J. Mabesoone, F. C. MacKintosh, P. H. J. Kouwer, and A. E. Rowan, Nature Commun. **5**, 5808 (2014).
[52] P. Olsson and S. Teitel, Phys. Rev. E **83**, 030302 (2011).
[53] X. Mao, A. Souslov, C. I. Mendoza, and T. C. Lubensky, Nature Commun. **6**, 5968 (2015).
[54] M. C. Wigbers, F. C. MacKintosh, and M. Dennison, Phys. Rev. E **92**, 042145 (2015).
[55] D. Nagy and P. Domokos, Phys. Rev. Lett. **115**, 043601 (2015).